Node diamond and face interpolated schemes for anisotropic diffusive equations

El Houssaine QUENJEL

Joint work with : P. Perre, & I. Turner, &A. Beljadid

Jean-Morlet Chair - Workshop: Discrete Duality Finite Volume Method and Applications
October 20, 2022

Outline

Outline

Anisotropic diffusion : - $\mathrm{div}\Lambda(x)\nabla u = f$

- Reservoir simulation : porous media flows.
- Chemotaxis models : Keller-Segel problems.
- Semi-conductor models.
- CFD models (Stokes, Navier-Stokes)
- ...

Hence, there is a strong interest in proposing "good" approximations of the diffusion.

Anisotropic diffusion : - $\mathrm{div}\Lambda(x)\nabla u = f$

A "good" approximation must take into account :

- Complex geometries of the domain
- Highly anisotropic tensors
- Stability & consistency
- ...

Benchmarks : FVCA5 '08, FVCA6 '11

Droniou's review, M3AS 2014

Outline

Ideas of the Node-diamond scheme

- The location of the diamonds (also for D.O.Fs)
- The gradient expression
- Decouple the cell unknowns from the vertex ones

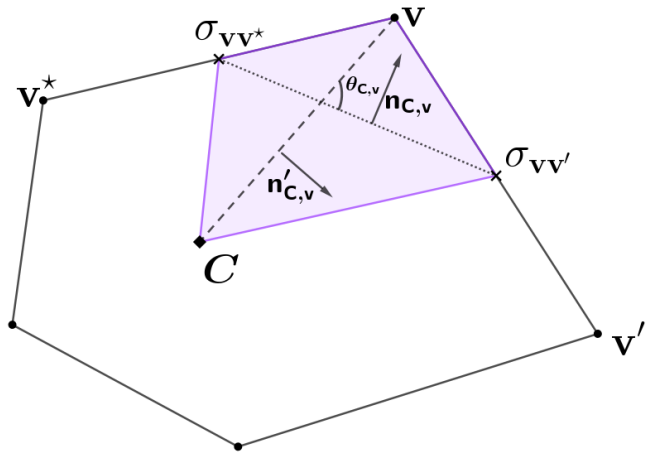

Figure: Given cell C of the mesh $\mathcal{T}$. The diamond $\mathcal{D}_{C,\mathbf{v}}$ is uniquely identified by C and the vertex $\mathbf{v}$.

From the DDFV discrete gradient

$$\nabla_{\mathcal{D}_{C,\mathbf{v}}} w_{\mathcal{M}} = \frac{1}{\sin(\theta_{\mathbf{C},\mathbf{v}})}\left(\frac{w_{\mathbf{v}} - w_C}{d_{C,\mathbf{v}}}\mathbf{n}_{\mathbf{C},\mathbf{v}} + \frac{w_{\sigma_{\mathbf{v}\mathbf{v}'}} - w_{\sigma_{\mathbf{v}\mathbf{v}^\star}}}{d'_{C,\mathbf{v}}}\mathbf{n}'_{\mathbf{C},\mathbf{v}}\right),$$

We substitute

$$w_{\sigma_{\mathbf{v}\mathbf{v}'}} = \frac{1}{2}(w_{\mathbf{v}} + w_{\mathbf{v}'}), \quad w_{\sigma_{\mathbf{v}\mathbf{v}^\star}} = \frac{1}{2}(w_{\mathbf{v}} + w_{\mathbf{v}^\star}), \tag{1}$$

to end up with

$$\nabla_{\mathcal{D}_{C,\mathbf{v}}} w_{\mathcal{M}} = \frac{1}{\sin(\theta_{\mathbf{C},\mathbf{v}})}\left(\frac{w_{\mathbf{v}} - w_C}{d_{C,\mathbf{v}}}\mathbf{n}_{\mathbf{C},\mathbf{v}} + \frac{1}{2}\frac{w_{\mathbf{v}'} - w_{\mathbf{v}^\star}}{d'_{C,\mathbf{v}}}\mathbf{n}'_{\mathbf{C},\mathbf{v}}\right). \tag{2}$$

2D Node-Diamond scheme

The scheme is derived from the discrete weak formulation

$$\int_\Omega \kappa_{h,\mathcal{T}} \nabla_h u_\mathcal{M} \cdot \nabla_h \varphi_\mathcal{M} \, \mathrm{d}x = \int_\Omega f \varphi_h \, \mathrm{d}x, \quad \forall \varphi_\mathcal{M} \in X_{\mathcal{M},0}. \tag{3}$$

The compact formulation (3) is quite helpful to carry out the scheme analysis. In the spirit of the gradient schemes formalism.
Then, the Node-Diamond scheme on T_C and $T_\mathbf{v}$

$$\sum_{\mathbf{v} \in \mathcal{S}_C} \left|\mathcal{D}_{C,\mathbf{v}}\right| \kappa_C \nabla_{\mathcal{D}_{C,\mathbf{v}}} u_\mathcal{M} \cdot \nabla_{\mathcal{D}_{C,\mathbf{v}}} \mathbf{1}_C = |T_C| \, f_{T_C} \quad \forall C \in \mathcal{T}, \tag{4}$$

$$\sum_{C \in \mathcal{T}_\mathbf{v}} \sum_{\nu \in \mathcal{S}_{C,\mathbf{v}}} \left|\mathcal{D}_{C,\mathbf{v}}\right| \kappa_C \nabla_{\mathcal{D}_{C,\nu}} u_\mathcal{M} \cdot \nabla_{\mathcal{D}_{C,\nu}} \mathbf{1}_\mathbf{v} = |T_\mathbf{v}| \, f_{T_\mathbf{v}} \quad \forall \mathbf{v} \in \mathcal{S} \setminus \mathcal{S}^D. \tag{5}$$

To include the Dirichlet boundary condition, one sets

$$u_\mathbf{v} = g_\mathbf{v}, \quad \forall \mathbf{v} \in \mathcal{S}^D. \tag{6}$$

We note that

$$\left|\mathcal{D}_{C,\mathbf{v}}\right| \kappa_C \nabla_{\mathcal{D}_{C,\mathbf{v}}} u_\mathcal{M} \cdot \nabla_{\mathcal{D}_{C,\mathbf{v}}} \mathbf{1}_C = \alpha_{C\mathbf{v}}(u_C - u_\mathbf{v}) + \beta_{C\mathbf{v}}(u_{\mathbf{v}^\star} - u_{\mathbf{v}'}),$$

where

$$\alpha_{C\mathbf{v}} = \frac{1}{2\left|\mathcal{D}_{C,\mathbf{v}}\right|}(d'_{C,\mathbf{v}})^2 \kappa_C \mathbf{n}_{\mathbf{C},\mathbf{v}} \cdot \mathbf{n}_{\mathbf{C},\mathbf{v}}, \quad \beta_{C\mathbf{v}} = \frac{1}{4\left|\mathcal{D}_{C,\mathbf{v}}\right|} d_{C,\mathbf{v}} d'_{C,\mathbf{v}} \kappa_C \mathbf{n}_{\mathbf{C},\mathbf{v}} \cdot \mathbf{n}'_{\mathbf{C},\mathbf{v}}.$$

Scheme analysis

Using similar tools from the DDFV framework, we proved

- Poincaré's inequality : $\|u_{\mathcal{M}}\|_0 \leq B_p \|u_{\mathcal{M}}\|_1$
- Energy estimate : $\|u_{\mathcal{M}}\|_1 \leq B$.
- Consistency of the discrete gradient : $\nabla_{h_\ell} u_{\mathcal{M}_\ell} \xrightarrow[\ell \to +\infty]{} \nabla u \quad \text{weakly} \quad \text{in } L^2(\Omega)^2$
- Strong convergence towards the weak solution

Extension to a nonlinear problem

Consider the unsteady diffusion problem

$$u - \nabla \cdot \varrho(u)\kappa(x)\nabla u = f \quad \text{in } \Omega, \tag{7}$$
$$u = g \quad \text{on } \partial\Omega, \tag{8}$$

It accounts for a main term in porous media and models of chemotaxis. ϱ is increasing from $\mathbb{R}^+$ to $\mathbb{R}^+$ with $\varrho(0) = 0$. A natural discretization of the main equation (7) can be given by

$$|T_C|\, u_C - \sum_{\mathbf{v}\in\mathcal{S}_C} |\mathcal{D}_{C,\mathbf{v}}|\, \varrho_{C,\mathbf{v}}(u_\mathcal{M})\kappa_C \nabla_{\mathcal{D}_{C,\mathbf{v}}} u_\mathcal{M} \cdot \nabla_{\mathcal{D}_{C,\mathbf{v}}} \mathbf{1}_C = |T_C|\, f_{T_C} \quad \forall C \in \mathcal{T}, \tag{9}$$
$$|T_\mathbf{v}|\, u_\mathbf{v} - \sum_{C\in\mathcal{T}_\mathbf{v}} \sum_{\nu\in\mathcal{S}_{C,\mathbf{v}}} |\mathcal{D}_{C,\mathbf{v}}|\, \varrho_{C,\mathbf{v}}(u_\mathcal{M})\kappa_C \nabla_{\mathcal{D}_{C,\nu}} u_\mathcal{M} \cdot \nabla_{\mathcal{D}_{C,\nu}} \mathbf{1}_\mathbf{v} = |T_\mathbf{v}|\, f_{T_\mathbf{v}} \quad \forall \mathbf{v} \in \mathcal{S}\setminus\mathcal{S}^D. \tag{10}$$

When $\mathbf{v} \in \mathcal{S}^D$ we enforce $u_\mathbf{v} = g_\mathbf{v}$. The only difference with the linear scheme is $\varrho_{C,\mathbf{v}}$ that is approximated by using the centered scheme

$$\varrho_{C,\mathbf{v}}(u_\mathcal{M}) = \frac{1}{4}\left(\varrho(u_c) + \varrho(u_\mathbf{v}) + \frac{\varrho(u_\mathbf{v}) + \varrho(u_{\mathbf{v}'})}{2} + \frac{\varrho(u_\mathbf{v}) + \varrho(u_{\mathbf{v}^\star})}{2}\right).$$

Up to some technicalities, similar convergence analysis holds true as in the linear case.

Comparison with the DDFV schemes

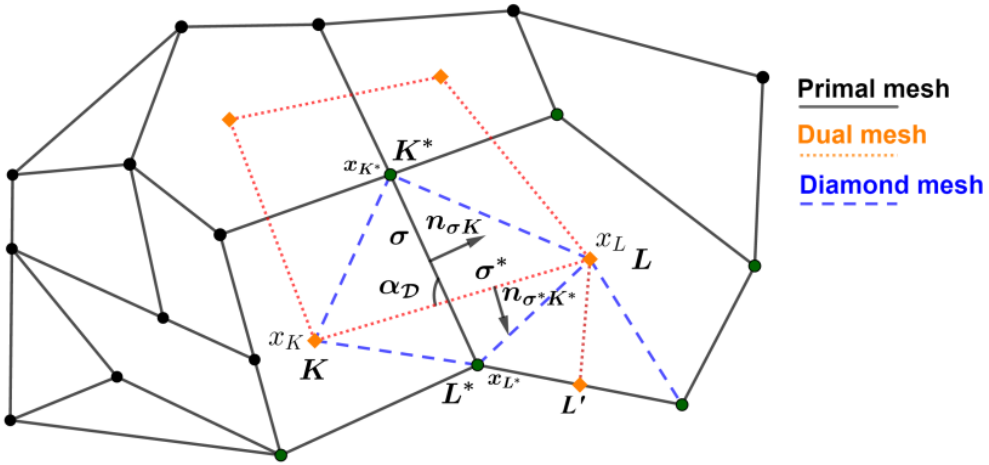

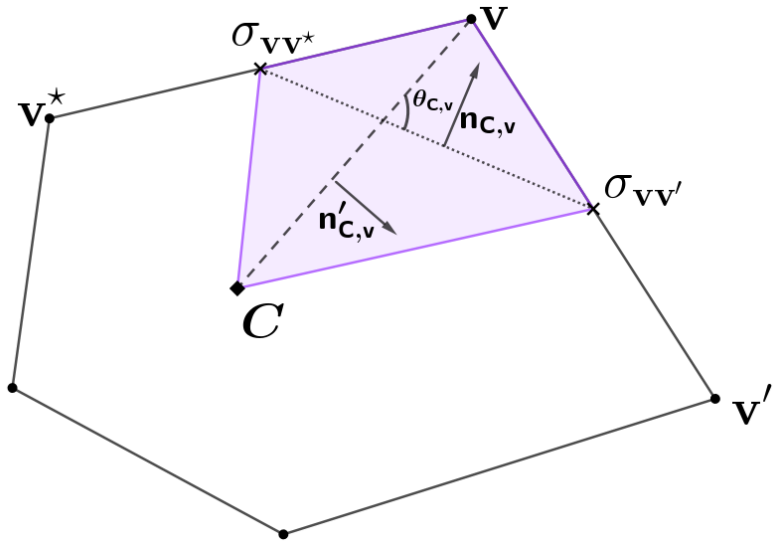

DDFV methodology

- A big diamond crossed by edge
- Not adequate to anisotropic $\Rightarrow$ m-DDFV method
- Conservation of the diffusive fluxes.
- Nodal + cell d.o.fs

Node-Diamond methodology

- Small diamonds.
- Handles naturally anisotropic tensor
- No conservation of the diffusive fluxes.
- Nodal d.o.fs after the elimination of the cell ones.

Case of additional convection

$$\overbrace{-\nabla\cdot\kappa(x)\nabla u}^{Node-Diamond}+\overbrace{\nabla\cdot u\mathbf{q}}^{Finite\ volume}=f \quad \text{in } \Omega, \tag{11}$$

$$u=g \quad \text{on } \partial\Omega, \tag{12}$$

$\mathbf{q}\in\mathcal{C}^1(\overline{\Omega},\mathbb{R}^2)$ and satisfy $\nabla\cdot\mathbf{q}\geq 0$. At the interface between T_C and $T_\mathbf{v}$, we set

$$\mathbf{q}_{C,\mathbf{v}}=\frac{1}{d'_{C,\mathbf{v}}}\int_{\sigma_{C,\mathbf{v}}}\mathbf{q}\cdot\mathbf{n}_{C,\mathbf{v}}\,\mathrm{d}s,\quad \boldsymbol{\mu_{C\mathbf{v}}}=\frac{d'_{C,\mathbf{v}}}{o_{C,\mathbf{v}}},\quad \boldsymbol{\mu_{\mathbf{v}C}}=\frac{d'_{C,\mathbf{v}}}{o_{C,\mathbf{v}}}\mu_C\left(-o_{C,\mathbf{v}}\mathbf{q}_{C,\mathbf{v}}\right).$$

Accordingly, the Node-Diamond scheme for steady convection-diffusion problems is written as

$$\sum_{\mathbf{v}\in\mathcal{S}_C}|\mathcal{D}_{C,\mathbf{v}}|\,\kappa_C\nabla_{\mathcal{D}_{C,\mathbf{v}}}u_\mathcal{M}\cdot\nabla_{\mathcal{D}_{C,\mathbf{v}}}\mathbf{1}_C+\sum_{\mathbf{v}\in\mathcal{S}_C}\left(\boldsymbol{\mu_{\mathbf{v}C}}u_C-\boldsymbol{\mu_{\mathbf{v}C}}u_\mathbf{v}\right)=|T_C|\,f_{T_C}\quad\forall C\in\mathcal{T},$$

$$\sum_{C\in\mathcal{T}_\mathbf{v}}\sum_{\nu\in\mathcal{S}_{C,\mathbf{v}}}|\mathcal{D}_{C,\mathbf{v}}|\,\kappa_C\nabla_{\mathcal{D}_{C,\nu}}u_\mathcal{M}\cdot\nabla_{\mathcal{D}_{C,\nu}}\mathbf{1}_\mathbf{v}-\sum_{C\in\mathcal{T}_\mathbf{v}}\alpha_{C\mathbf{v}}\left(\boldsymbol{\mu_{\mathbf{v}C}}u_C-\boldsymbol{\mu_{\mathbf{v}C}}u_\mathbf{v}\right)=|T_\mathbf{v}|\,f_{T_\mathbf{v}}\quad\forall\mathbf{v}\in\mathcal{S}\setminus\mathcal{S}^D,$$

$$u_\mathbf{v}=g_\mathbf{v},\quad\forall\mathbf{v}\in\mathcal{S}^D. \tag{13}$$

(i) **Upwind scheme** : $\mu_C(a)=\max(a,0)$.

(ii) **Scharfetter–Gummel scheme** :

$$\mu_C(a)=\min(1,\lambda_{\kappa_C})\mu_{\mathrm{sg}}\left(\frac{a}{\min(1,\lambda_{\kappa_C})}\right),\quad\mu_{\mathrm{sg}}(s)=\frac{-s}{e^{-s}-1}-1,\ s\neq 0,\ \mu_{\mathrm{sg}}(0)=0.$$

Implementation and resolution $\mathbf{A}u_{\mathcal{M}} = \mathbf{b}_{\mathcal{M}}$

For assembling $\mathbf{A}$, consider the cell-vertex $(C \to \mathbf{v})$ and the vertex-vertex $(\mathbf{v}^\star \to \mathbf{v}')$ contributions

$$F_{C,\mathbf{v}} = \alpha_{C\mathbf{v}}(u_C - \mathbf{Id}_{\mathbf{v}} u_{\mathbf{v}}) + \beta_{C\mathbf{v}}(\mathbf{Id}_{\mathbf{v}^\star} u_{\mathbf{v}^\star} - \mathbf{Id}_{\mathbf{v}'} u_{\mathbf{v}'}),$$
$$F_{\mathbf{v}^\star,\mathbf{v}'} = \alpha'_{\mathbf{v}C}(u_{\mathbf{v}^\star} - \mathbf{Id}_{\mathbf{v}'} u_{\mathbf{v}'}) + \beta_{C\mathbf{v}}(u_C - \mathbf{Id}_{\mathbf{v}} u_{\mathbf{v}}), \quad \mathbf{v}^\star \in \mathcal{S}_C \setminus \mathcal{S}^D,$$

where

$$\alpha_{C\mathbf{v}} = \frac{1}{2\,|\mathcal{D}_{C,\mathbf{v}}|}(d'_{C,\mathbf{v}})^{\mathbf{2}} \kappa_C \mathbf{n}_{\mathbf{C},\mathbf{v}} \cdot \mathbf{n}_{\mathbf{C},\mathbf{v}}, \quad \beta_{C\mathbf{v}} = \frac{1}{4\,|\mathcal{D}_{C,\mathbf{v}}|} d_{C,\mathbf{v}} d'_{C,\mathbf{v}} \kappa_C \mathbf{n}_{\mathbf{C},\mathbf{v}} \cdot \mathbf{n}'_{\mathbf{C},\mathbf{v}},$$
$$\alpha'_{C\mathbf{v}} = \frac{1}{8\,|\mathcal{D}_{C,\mathbf{v}}|} d^{\mathbf{2}}_{C,\mathbf{v}} \kappa_C \mathbf{n}'_{\mathbf{C},\mathbf{v}} \cdot \mathbf{n}'_{\mathbf{C},\mathbf{v}}.$$

The contribution vertex-cell $(\mathbf{v} \to C)$ is filled by symmetry $F_{\mathbf{v},C} = -F_{C,\mathbf{v}}$ as long as $\mathbf{v} \notin \mathcal{S}^D$. Similarly to $(\mathbf{v}' \to \mathbf{v}^\star)$. The structure of the final stiffness matrix is composed of four blocks

$$\mathbf{A} = \begin{pmatrix} \mathbf{A}_{\mathcal{S}} & \mathbf{A}_{\mathcal{S},\mathcal{T}} \\ \mathbf{A}_{\mathcal{T},\mathcal{S}} & \mathbf{A}_{\mathcal{T}} \end{pmatrix}.$$

The block $\mathbf{A}_{\mathcal{T}}$ is an invertible diagonal matrix. Apply the Schur complement to eliminate the cell unknowns before the resolution process. This amounts to solving

$$\left(\mathbf{A}_{\mathcal{S}} - \mathbf{A}_{\mathcal{S},\mathcal{T}} \mathbf{A}_{\mathcal{T}}^{-1} \mathbf{A}_{\mathcal{T},\mathcal{S}}\right) u_{\mathcal{S}} = \mathbf{b}_{\mathcal{S}} - \mathbf{A}_{\mathcal{S},\mathcal{T}} \mathbf{A}_{\mathcal{T}}^{-1} \mathbf{b}_{\mathcal{T}}.$$

Finally, one update

$$u_{\mathcal{T}} = \mathbf{A}_{\mathcal{T}}^{-1}\left(\mathbf{b}_{\mathcal{T}} - \mathbf{A}_{\mathcal{T},\mathcal{S}} u_{\mathcal{S}}\right).$$

Results : various polygonal meshes (distorted, non-conform, ...)

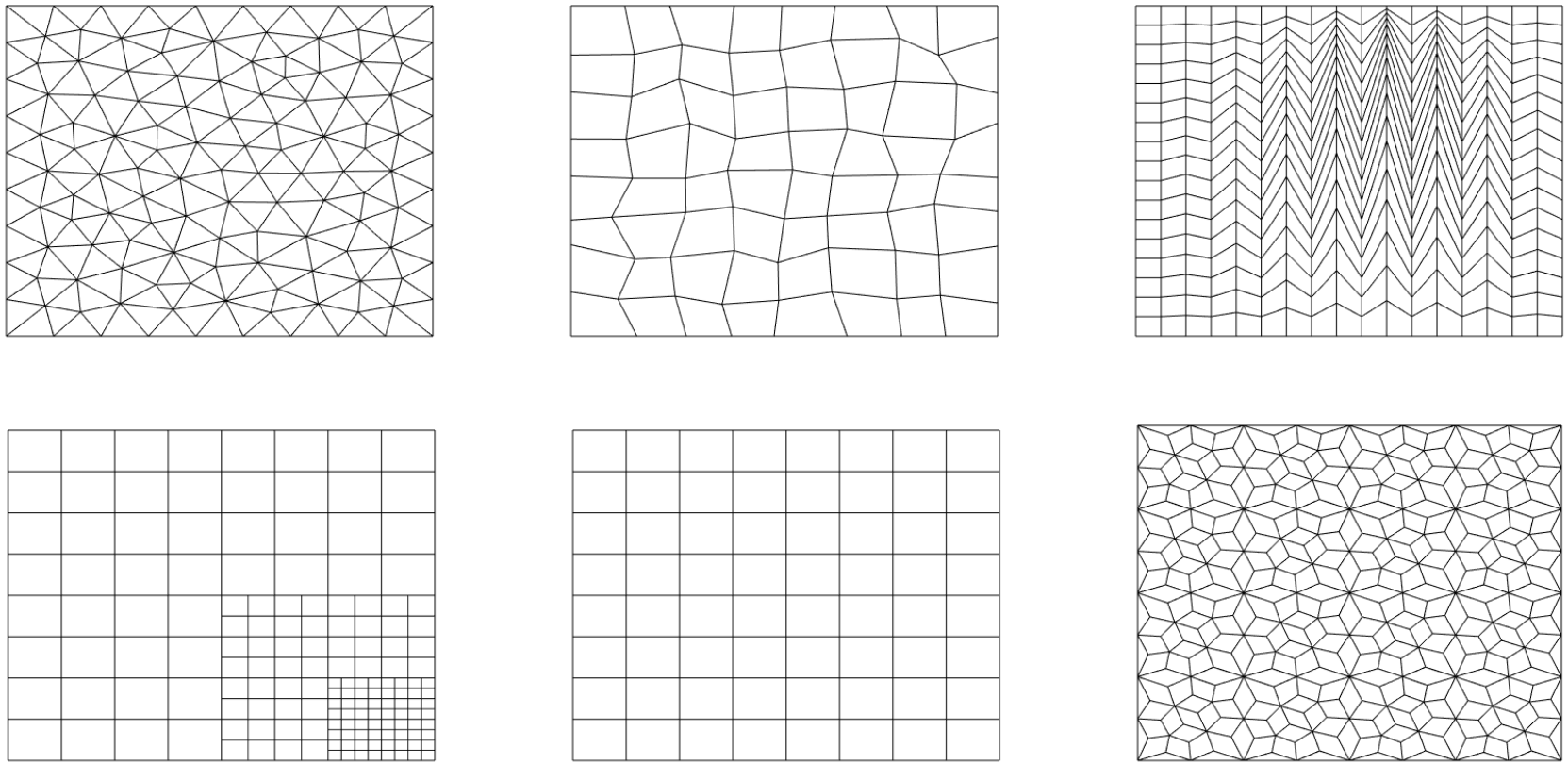

Figure: From left to right: Cartesian, triangular, random, locally refined, Kershaw, and diamond meshes.

Results : case of heterogeneous rotating anisotropy

Consider

$$u_e(x) = \sin(\pi x_1)\sin(\pi x_2), \quad x = (x_1, x_2) \in \Omega.$$

The boundary condition agrees with u_e. The source term is determined from

$$\kappa(x) = \begin{pmatrix} \varepsilon \widehat{x}_1^2 + \widehat{x}_2^2 & -(1-\varepsilon)\widehat{x}_1\widehat{x}_2 \\ -(1-\varepsilon)\widehat{x}_1\widehat{x}_2 & \widehat{x}_1^2 + \varepsilon \widehat{x}_2^2 \end{pmatrix},$$

where we set $\widehat{x}_1 = x_1 - 0.1$ and $\widehat{x}_2 = x_2 - 0.1$. The parameter ε is equal to 10^{-3}.

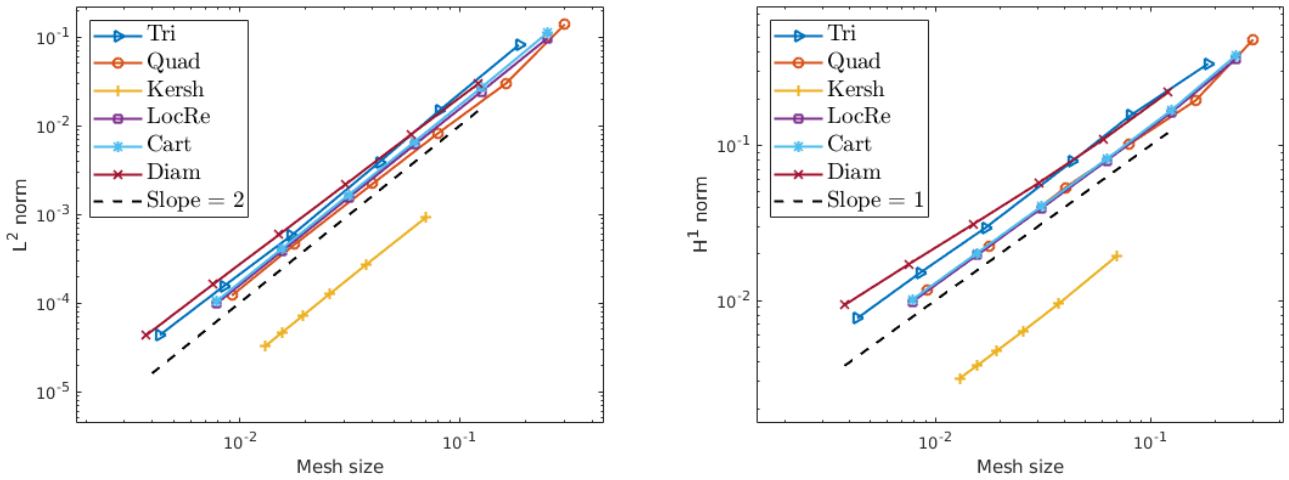

Figure: Errors in L^2-norm (left) and H^1-norm (right) with a heterogeneous rotating anisotropy.

	Tri	Quad	Kersh	LocRef	Cart	Diam
$u_{\min}$	-0.0199	0.0000	0.0000	0.0000	0.0000	-0.0384
$u_{\max}$	1.0774	1.1301	1.0000	1.1166	1.1390	0.9986

Table: DMP on the first element of each mesh category.

Results : oblique flow

This test-case is taken from the FVCA5 benchmark with the same set up. The diffusion tensor is

$$\kappa(x) = \mathcal{R}(\theta) \times \begin{pmatrix} 1 & 0 \\ 0 & 0.001 \end{pmatrix} \times \mathcal{R}^{-1}(\theta), \quad \text{and} \quad \mathcal{R}(\theta) = \begin{pmatrix} \cos(\theta) & -\sin(\theta) \\ \sin(\theta) & \cos(\theta) \end{pmatrix},$$

where the rotation angle is $\theta = 40$ degrees. The source function f is set to 0. The Dirichlet boundary condition is prescribed by the piecewise linear continuous function

$$u_e(x) = \begin{cases} 1 & \text{on } (0, 0.2) \times \{0\} \bigcup \{0\} \times (0, 0.2) \\ 0 & \text{on } (0.8, 1) \times \{1\} \bigcup \{1\} \times (0.8, 1) \\ 0.5 & \text{on } (0.3, 1) \times \{0\} \bigcup \{0\} \times (0.3, 1) \\ 0.5 & \text{on } (0, 0.7) \times \{1\} \bigcup \{1\} \times (0, 0.7) \end{cases}.$$

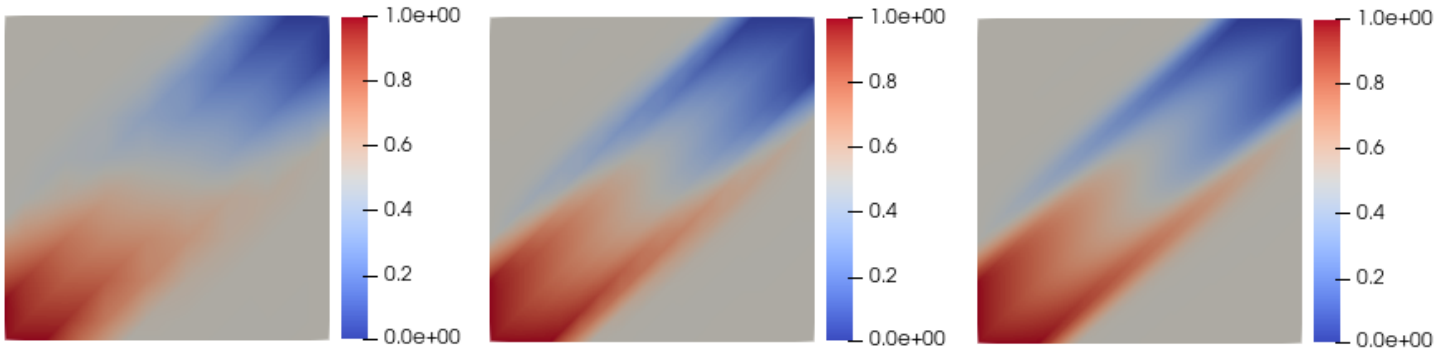

Figure: Test 3 : from left to right : approximate solution of the oblique flow test-case on three Cartesian meshes ($\mathbf{Cart_2}$, $\mathbf{Cart_3}$ and $\mathbf{Cart_4}$).

The obtained total energy behaves like in the FVCA benchmark.

Outline

Anisotropic diffusion : - $\mathrm{div}\Lambda(x)\nabla u = f$

The aim is to propose a scheme with the following strengths

- Handle Hexahedral geometries
- Deal with Highly anisotropic tensors
- Ensure Stability & consistency
- Use of purely nodal unknowns without additional ones

Applications : prediction of macroscopic properties of materials, heat transfer in wood

Scheme's idea

Set : $\overrightarrow{\tau_{\mathcal{F}_{2i-1}\mathcal{F}_{2i}}} = \overrightarrow{x_{\mathcal{F}_{2i-1}}x_{\mathcal{F}_{2i}}}$. The DDFV gradient writes

$$\nabla_K u_{\mathcal{T}} = \frac{1}{|K|}\Big((u_{\mathcal{F}_2} - u_{\mathcal{F}_1})\overrightarrow{N_{12}} + (u_{\mathcal{F}_4} - u_{\mathcal{F}_3})\overrightarrow{N_{34}} + (u_{\mathcal{F}_6} - u_{\mathcal{F}_5})\overrightarrow{N_{56}} \Big), \tag{14}$$

where

$$\overrightarrow{N_{12}} = \overrightarrow{\tau_{\mathcal{F}_3\mathcal{F}_4}} \wedge \overrightarrow{\tau_{\mathcal{F}_5\mathcal{F}_6}}, \quad \overrightarrow{N_{34}} = \overrightarrow{\tau_{\mathcal{F}_5\mathcal{F}_6}} \wedge \overrightarrow{\tau_{\mathcal{F}_1\mathcal{F}_2}}, \quad \overrightarrow{N_{56}} = \overrightarrow{\tau_{\mathcal{F}_1\mathcal{F}_2}} \wedge \overrightarrow{\tau_{\mathcal{F}_3\mathcal{F}_4}}.$$

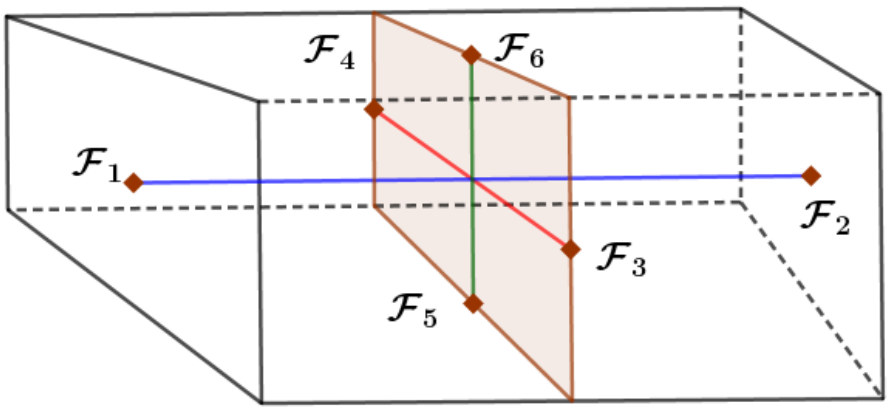

Figure: opposite faces in the cell K and their corresponding directions.

The scheme becomes nodal by taking $u_{\mathcal{F}_i} = \frac{1}{4}\sum_{s\in\mathcal{T}_{\mathcal{F}_i}} u_s$.

Scheme's idea

Set : $\overrightarrow{\tau_{\mathcal{F}_{2i-1}\mathcal{F}_{2i}}} = \overrightarrow{x_{\mathcal{F}_{2i-1}}x_{\mathcal{F}_{2i}}}$. The DDFV gradient writes

$$\nabla_K u_{\mathcal{T}} = \frac{1}{|K|}\Big((u_{\mathcal{F}_2} - u_{\mathcal{F}_1})\overrightarrow{N_{12}} + (u_{\mathcal{F}_4} - u_{\mathcal{F}_3})\overrightarrow{N_{34}} + (u_{\mathcal{F}_6} - u_{\mathcal{F}_5})\overrightarrow{N_{56}}\Big), \tag{15}$$

where

$$\overrightarrow{N_{12}} = \overrightarrow{\tau_{\mathcal{F}_3\mathcal{F}_4}} \wedge \overrightarrow{\tau_{\mathcal{F}_5\mathcal{F}_6}}, \quad \overrightarrow{N_{34}} = \overrightarrow{\tau_{\mathcal{F}_5\mathcal{F}_6}} \wedge \overrightarrow{\tau_{\mathcal{F}_1\mathcal{F}_2}}, \quad \overrightarrow{N_{56}} = \overrightarrow{\tau_{\mathcal{F}_1\mathcal{F}_2}} \wedge \overrightarrow{\tau_{\mathcal{F}_3\mathcal{F}_4}}.$$

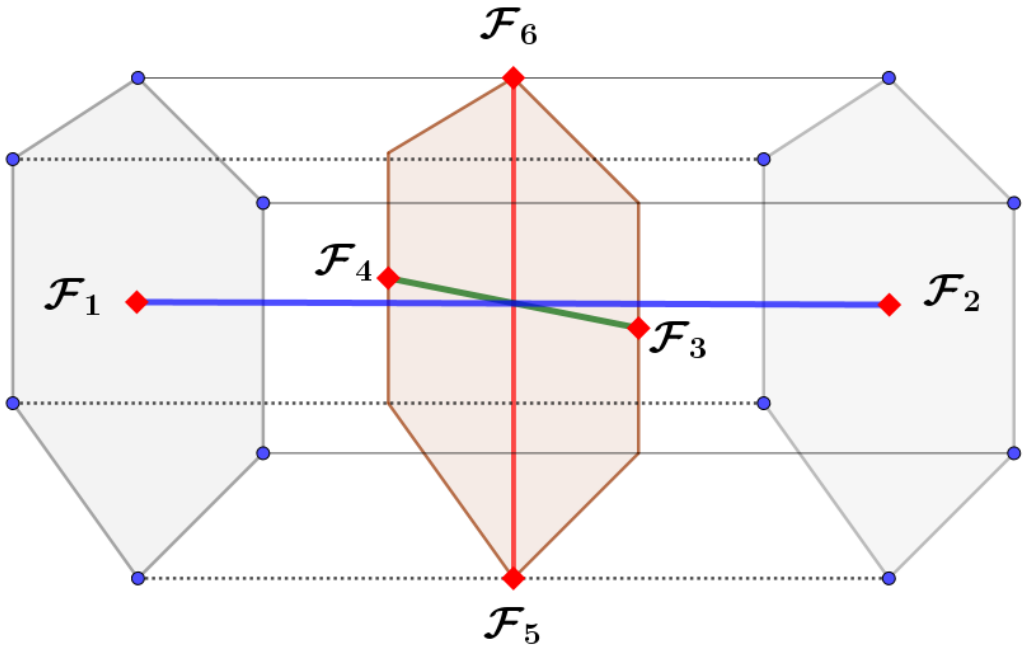

Figure: opposite faces in the cell K and their corresponding directions.

The scheme becomes nodal by taking $u_{\mathcal{F}_i} = \frac{1}{4}\sum_{s\in\mathcal{T}_{\mathcal{F}_i}} u_s, i = 1,2,3,4.$ $u_{\mathcal{F}_5} = u_{s_5}$, $u_{\mathcal{F}_6} = u_{s_6}$

Mesh used for the numerical results

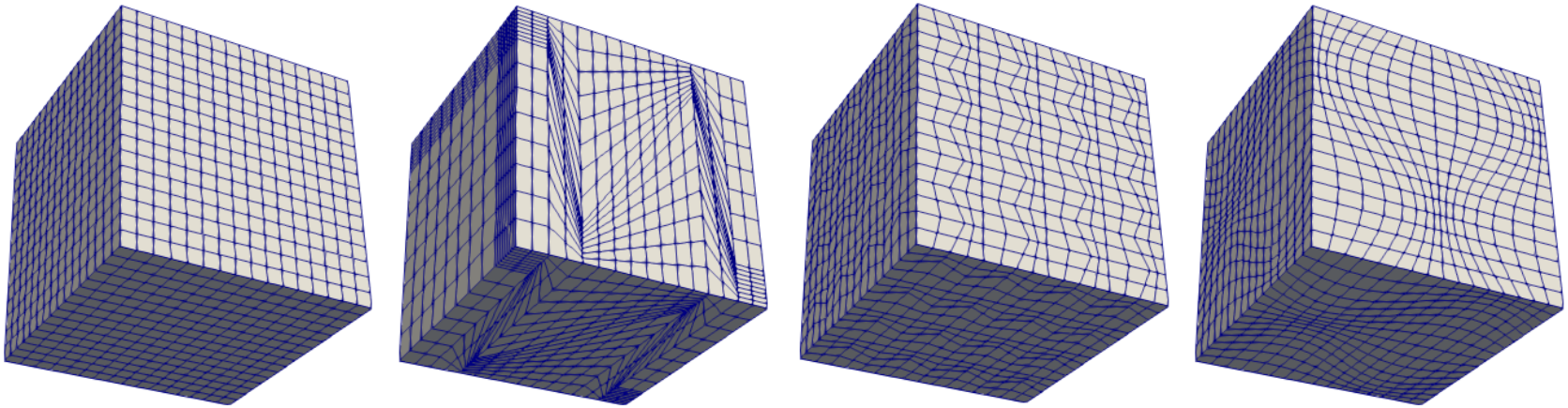

Figure: Cartesian, Kershaw, fluctuated and sinusoidal meshes.

Mesh Nb	Nb of DOFs	Nb NzCoefffMat	Density
1	729	15625	2.94011 %
2	4913	117649	0.48741 %
3	35937	912673	0.07066 %
4	274625	7189057	0.00953 %
5	2097152	57066625	0.00129 %

Table: DOFs for each mesh and the corresponding number of non zero coefficients of the stiffness matrix.

Results

In this test, the eigenvectors directions change over the domain

$$\Lambda(x,y,z) = \mathcal{R}_\theta(x) \times \begin{pmatrix} 1 & 0 & 0 \\ 0 & \varepsilon & 0 \\ 0 & 0 & \eta(1+x+y+z) \end{pmatrix} \times \mathcal{R}_\theta(x)^t,$$

where $\varepsilon = 0.1$, $\eta = 10$ and

$$\mathcal{R}_\theta(x) = \begin{pmatrix} \cos(\pi x) & -\sin(\pi x) & 0 \\ \sin(\pi x) & \cos(\pi x) & 0 \\ 0 & 0 & 1 \end{pmatrix}.$$

We impose the exact solution to be

$$u_e(x,y,z) = \sin(\pi x)\sin(\pi x)\sin(\pi z).$$

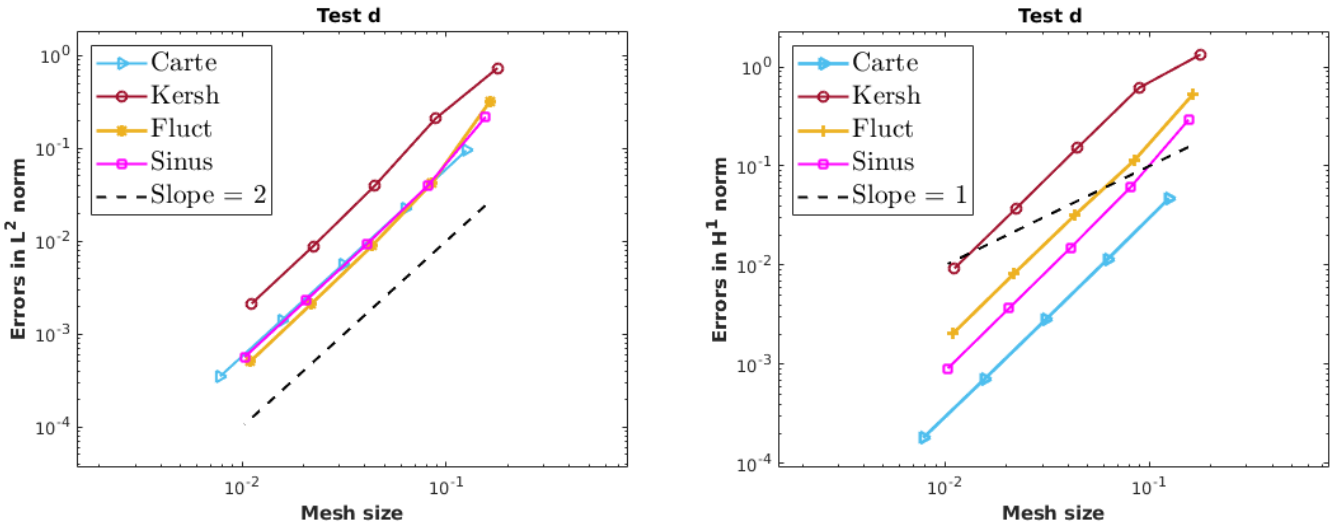

Figure: Numerical relative errors in the L^2-norm (left) and H^1-norm (right).

Solver behavior : Conjugate Gradient + SSOR preconditioner

Cartesian meshes								
$h_{\mathcal{T}}$	κ	$\kappa^\star$	$\lambda_{\max}$	$\lambda^\star_{\max}$	#it	#it*	CPU	CPU*
0.125	2.47E+3	8.74E+1	1.22E+1	1.01E+0	66	27	0.0254	0.0153
0.063	2.69E+4	6.68E+2	7.43E+0	1.02E+0	46	18	0.1849	0.0905
0.031	4.53E+5	6.96E+3	4.17E+0	1.05E+0	74	14	1.4793	1.0899
Kershaw meshes								
$h_{\mathcal{T}}$	κ	$\kappa^\star$	$\lambda_{\max}$	$\lambda^\star_{\max}$	#it	#it*	CPU	CPU*
0.178	3.35E+3	5.72E+1	2.42E+1	1.10E+0	145	43	0.0321	0.0209
0.089	6.90E+4	2.22E+2	2.46E+1	1.05E+0	618	98	0.3600	0.1235
0.045	1.59E+6	1.08E+3	1.73E+1	1.12E+0	1017	111	3.8786	1.1868
Fluctuated meshes								
$h_{\mathcal{T}}$	κ	$\kappa^\star$	$\lambda_{\max}$	$\lambda^\star_{\max}$	#it	#it*	CPU	CPU*
0.163	3.49E+3	6.30E+1	1.66E+1	9.95E-1	131	37	0.0377	0.0211
0.085	7.39E+4	6.56E+2	1.32E+1	1.11E+0	342	64	0.2631	0.1088
0.043	1.41E+6	2.02E+3	8.68E+0	1.05E+0	284	44	2.1575	1.0610
Sinusoidal meshes								
$h_{\mathcal{T}}$	κ	$\kappa^\star$	$\lambda_{\max}$	$\lambda^\star_{\max}$	#it	#it*	CPU	CPU*
0.156	5.63E+3	6.63E+1	1.92E+1	1.08E+0	145	32	0.0294	0.0172
0.081	9.43E+4	5.74E+2	1.53E+1	1.05E+0	152	31	0.2138	0.1063
0.041	1.69E+6	1.96E+3	1.01E+1	1.13E+0	162	26	1.7939	0.9587

Table: solver statistics before and after the preconditioning.

Outline

Conclusion & perspectives

- Overview on the face interpolated methods
- Link with the DDFV methods
- A particular emphasis is set on the approximation of the gradient.

- Application to complex two-phase flows in porous media.
- Prediction of macroscopic properties of wood
- Heat transfer in hygroscopic media (wood, fibers, ...)

Non-exhaustive references

E. H. Quenjel, and A. Beljadid

Node-Diamond approximation of heterogeneous and anisotropic diffusion systems on arbitrary two-dimensional grids MATCOM, 204, 450-472, 2023.

E. H. Quenjel, P. Perré, and I. Turner

A 3D face interpolated discretisation method for simulating highly anisotropic diffusive processes on general hexahedral meshes. Preprint, 2022.

J. Droniou, R. Eymard, T. Gallouët, C. Guichard, and R. Herbin.

The gradient discretisation method.Volume 82. Springer, 2018.

Andreianov, B., M. Bendahmane, F. Hubert, and S. Krell. 2012.

On 3D DDFV discretization of gradient and divergence operators. I. Meshing, operators and discrete duality. IMA JNA 32 (4): 1574–1603, 2012 .

B. Da Veiga, J. Droniou, and G. Manzini

A unified approach for handling convection terms in FV and mimetic discretization methods for elliptic problems. IMA JNA, 31(4):1357–1401, 2011.

Coudière, Y., C. Pierre, O. Rousseau, and R. Turpault. 2009.

A 2D/3D discrete duality finite volume scheme. Application to ECG simulation, 6 (1): 24, 2009 .

B. Andreianov, F. Boyer, and F. Hubert

DDFV schemes for Leray–Lions– type elliptic problems on general 2D meshes. Numerical Methods for PDEs, 23(1):145–195, 2007.

K. Domelevo, and P. Omnes

A finite volume method for the Laplace equation on almost arbitrary two-dimensional grids. ESAIM M2AN, 39(6), 1203–1249, 2005.

Thank you for your attention !